

Paleoceanography and Paleoclimatology

RESEARCH ARTICLE

10.1029/2019PA003580

Key Points:

- The AMOC stability is associated with the strength of the North Atlantic westerlies, not with the mean AMOC strength
- An unstable AMOC features a small but not strictly negative overturning freshwater transport, and a weak AMOC/density gradient relationship
- By comparing with ΔSST (LGM-PI) proxies, the best model fit suggests that the LGM had stronger winds and weaker vertical mixing/AMOC (~13 Sv)

Supporting Information:

- Supporting Information S1

Correspondence to:

M. Goes,
marlos.goes@noaa.gov

Citation:

Goes, M., Murphy, L. N., & Clement, A. C. (2019). The stability of the AMOC during Heinrich events is not dependent on the AMOC strength in an Intermediate Complexity Earth System model ensemble. *Paleoceanography and Paleoclimatology*, 34, 1359–1374.
<https://doi.org/10.1029/2019PA003580>

Received 1 FEB 2019

Accepted 1 AUG 2019

Accepted article online 6 AUG 2019

Published online 20 AUG 2019

The Stability of the AMOC During Heinrich Events Is Not Dependent on the AMOC Strength in an Intermediate Complexity Earth System Model Ensemble

Marlos Goes^{1,2} , Lisa N. Murphy³ , and Amy C. Clement³ 

¹Cooperative Institute for Marine and Atmospheric Studies, University of Miami, Miami, FL, USA, ²Atlantic Oceanographic and Meteorological Laboratory, NOAA, Miami, FL, USA, ³Rosenstiel School of Marine and Atmospheric Science, University of Miami, Miami, FL, USA

Abstract Previous studies that used Earth system models of intermediate complexity showed that stronger background winds drove a more vigorous and stable Atlantic Meridional Overturning Circulation (AMOC), while those with weaker winds had a more sluggish and unstable AMOC. In other studies, ensembles under vertical mixing uncertainty showed the opposite effect, where the simulations with a stronger AMOC were more unstable. To tackle this conundrum, we produce a model ensemble featuring uncertainties related to wind forcing and vertical mixing to understand the role of feedbacks on the AMOC stability. We show that the stability of the AMOC is not influenced by vertical mixing and the AMOC strength, and rather, it is determined by the strength of the Northern Hemisphere winds. Paleoproxies indicate an AMOC shutdown during the last Heinrich Stadial. Our comparisons to sea surface temperature proxies show a better fit with the simulations under a stable AMOC, which corresponds to a forced off-state. The sign of the AMOC-driven freshwater transport in the South Atlantic, which is regarded as an index for its stability, is shown not to be an absolute measure, although its evolution agrees with the salt advection feedback.

Plain Language Summary Information on the structure of the Atlantic Meridional Overturning Circulation (AMOC) during the Last Glacial Maximum (LGM) and its behavior during strong freshwater discharge in the Northern Hemisphere (NH) associated with Heinrich Stadials are subject to deep uncertainty. In this study, we use an intermediate complexity Earth System model to examine the influence of the mean AMOC strength and wind forcing on the AMOC behavior during the LGM and Heinrich Stadial 1. Our results show that it is the strength of the NH winds, and not the mean AMOC strength, that determines the stability of the AMOC during periods of freshwater discharge. Stronger NH winds maintains a stable AMOC (one that recovers when freshwater discharge terminates), increases the upper ocean stratification, cools the ocean, and decreases Arctic ice coverage. Stronger stratification increases the AMOC sensitivity to the meridional density gradient, which is mostly driven by salinity effects in the LGM. Simulations that show a bistable AMOC, in which it remains shutdown after collapse, present a weak meridional overturning freshwater transport, but not necessarily negative, which may impact the use of this index as a stability indicator.

1. Introduction

Proxy data in the North Atlantic indicate that there were abrupt changes in the Atlantic Meridional Overturning Circulation (AMOC) during the last glacial period (Broecker et al., 1992; Dansgaard et al., 1993). The strength of the AMOC during the Last Glacial Maximum (LGM) is still contested with proxy records indicating both a weaker or more vigorous but shallower cell (McManus et al., 2004; Lippold et al., 2012; Gherardi et al., 2009; Böhm et al., 2015). In contrast, the most recent climate models that participated in the Paleoclimate Model Intercomparison Project Phase 3 (PMIP3) showed that when forced with LGM boundary conditions they generally have a stronger and deeper AMOC (Muglia & Schmittner, 2015). The stronger modeled LGM AMOC was attributed to stronger Northern Hemisphere westerly wind likely resulting from the North American ice sheet and interactions with sea ice (Oka et al., 2012; Sherriff-Tadano et al., 2018). This uncertainty in the mean state of the AMOC impacts how the deglacial ocean responded to freshwater input (Weber et al., 2007). During the deglaciation, AMOC indicators show a much weaker or even shut down circulation during Heinrich Stadial 1 (HS1; ~18–15 ka BP; McManus et al., 2004;

Oppo et al., 2015, among others). Freshwater discharge into the North Atlantic is believed to have driven this change, which is corroborated in modeling studies (Manabe & Stouffer, 1988; Stommel, 1961). However, this driver has recently been questioned (Barker et al., 2015) on the grounds that the freshwater discharge from iceberg calving followed rather than preceded the cooling in the North Atlantic. How the AMOC responds to freshwater forcing during past periods of abrupt climate change and future climate change is still highly uncertain. This is partly due to the uncertainties about the amount of freshwater discharge in the North Atlantic (Roche et al., 2014; Sévellec et al., 2017) and also may be dependent on the stability of the AMOC itself, and whether it is monostable (i.e., one with strong overturning in the North Atlantic) or bistable (i.e., one with two stable states with either strong or weak overturning in the North Atlantic), which is still a matter of debate (Garzoli et al., 2013; Liu et al., 2017). This has large implications on how the AMOC responds to and recovers from freshwater forcing.

Following the framework of Stommel (1961), indicators have been created to infer the stability of the AMOC in climate models. These indicators are mostly related to the freshwater convergence in the Atlantic basin (Liu et al., 2014,b), which can be approximated to a large extent as the sign of AMOC-driven freshwater transport (M_{ov}) into the South Atlantic at $\sim 34^{\circ}\text{S}$ (e.g., Huisman et al., 2010; Rahmstorf, 1996). Although the sign of the present-day M_{ov} at 34°S estimated from observations is negative (e.g., Garzoli et al., 2013; Gent, 2018; Goes et al., 2018), suggesting freshwater divergence in the Atlantic Ocean and a bistable AMOC, the accuracy of this indicator has been recently challenged, since it relies on many assumptions about the role of the gyre and recirculations, vertical structure, air-sea-ice interaction, and eddies on the freshwater transport (e.g., Gent, 2018; Cheng et al., 2018).

Intermediate complexity models can represent two states of the AMOC, but more complex climate models generally fail to represent this feature (Bryden et al., 2011; Drijfhout et al., 2011; Gent, 2018; Liu, Liu, & Brady, 2014; Weber et al., 2007; Weijer et al., 1999). This contrast can be due, for example, to biases in the ocean freshwater content (Liu, Liu, Cheng, & Hu, 2014; Mecking et al., 2017; Weber & Drijfhout, 2007) or due to atmospheric forcing and air-sea interaction uncertainty (Large & Danabasoglu, 2006; Murphy et al., 2017; Gent, 2018). Previous studies associate model biases in the tropical and North Atlantic with the mean state of the AMOC (Wang et al., 2014). In addition, the transient response of the AMOC to external (heat and freshwater) forcing has also been linked to its mean state, that is, models with a stronger AMOC tend to show a greater and more stable decline (Kostov et al., 2014; Newsom et al., 2016; Weaver et al., 2007; Xie & Vallis, 2012), whereas models with a weaker AMOC generally show a smaller weakening of the deep convection in the polar regions (He et al., 2017; Rugenstein et al., 2013), consistent with the fact that a control simulation with a weaker AMOC is more stable since the North Atlantic is colder and there is more extensive North Atlantic ice coverage (Levermann et al., 2007; Saenko et al., 2004). Therefore, such stability biases could also be related to the mean state of the AMOC.

Our main question is as follows: What is the effect of the mean AMOC strength on the stability of the AMOC? Two frameworks can be used to test whether the stability of the AMOC is related to its strength: by examining model structure (i.e., multimodel ensemble) or by examining model parameters (monomodel ensemble). Analyzing parametric uncertainty rather than structural (multimodel) uncertainties may provide a more parsimonious framework to understand the processes underlying the AMOC stability. Using an intermediate complexity Earth System model under a realistic range of freshwater hosing experiments for HS1 (Roche et al., 2014), Murphy et al. (2017) could reproduce two different states of the AMOC, a monostable and a bistable state, by changing the strength of the background climatological winds. Additionally, when the winds were stronger the mean AMOC was much stronger relative to the simulations with weaker winds (22 Sv versus 13 Sv). To address the question posed above, we expand the Murphy et al. (2017) analysis by including AMOC strength uncertainty. This is done by including vertical mixing parametric uncertainty, which is a highly uncertain parameter in low resolution ocean models and previous studies have shown that the AMOC is extremely sensitive to it (Sijp & England, 2006).

2. Materials and Methods

2.1. Model Description

The University of Victoria Earth System Climate Model (UVic ESCM) version 2.9 is used to analyze the behavior of the AMOC under LGM boundary conditions. UVic consists of a coupled system with a three-

dimensional ocean general circulation model, a dynamic thermodynamic sea ice model, a simple one-layer energy-moisture balance model of the atmosphere (Weaver et al., 2001), and MOSES-TRIFFID land-surface and dynamic terrestrial vegetation components (Meissner et al., 2003). The atmosphere calculates surface heat and freshwater fluxes without flux correction and includes a variable latitudinal atmospheric diffusion of heat and moisture advection, which results in a much better fit to high-latitude LGM temperatures proxies (Fyke & Eby, 2012). The ocean model is based on the Geophysical Fluid Dynamics Laboratory Modular Ocean Model 2.2 (Pacanowski, 1995) with a global resolution of 1.8° (meridional) by 3.6° (zonal) and has 19 layers in the vertical. Eddy mixing parameterization follows Gent and McWilliams (1990), and the ocean vertical diffusivity is parameterized using the Bryan and Lewis (1979) vertical distribution. The sea ice component incorporates an elastic-viscous-plastic rheology to represent sea ice dynamics and various options for the representation of sea ice thermodynamics and thickness distribution (Bitz et al., 2001).

The LGM boundary conditions correspond to 19-Kyr orbital parameters (Braconnot et al., 2007), ice sheets, and atmospheric CO₂ baseline of ~ 190 ppm in a coupled carbon cycle model between atmosphere, ocean, and land. Continental boundaries are kept the same as present day, which in UVic has a closed Bering Strait.

2.2. Wind Forcing

The standard UVic model is forced with prescribed climatological winds from the National Center for Environmental Research (National Centers for Environmental Prediction; Kalnay et al., 1996) and uses a dynamical wind feedback scheme, in which winds are allowed to change using a geostrophic/diffusive approximation in response to sea surface pressure anomalies (Fanning & Weaver, 1997; Weaver et al., 2001). The sea surface pressure anomalies are calculated from temperature differences between our LGM control simulation and a long present-day control simulation. These geostrophic wind anomalies are then added as a perturbation to the prescribed mean wind/wind stress fields.

Following the methodology described in Goes et al. (2014) and Murphy et al. (2017), uncertainty in wind forcing is accounted for by prescribing two different background winds (see Figure S1a in the supporting information): (i) standard “UVic” LGM winds, which incorporates LGM anomalies relative to the prescribed National Centers for Environmental Prediction Present Day (PD) climatological winds, and (ii) “CAM” LGM winds, in which the climatological LGM-Preindustrial (PI) wind anomalies from simulations of the National Center for Atmospheric Research Community Climate System Model version 4 are used. In the CAM winds simulations, instead of prescribing the winds directly, we prescribed Community Climate System Model version 4 LGM-PI sea level pressure anomalies to the model climatological state. After a long spin-up period ($>3,000$ years, and branching from equilibrated runs), outputs from the last 100 years are used to replace the background climatological state of winds, wind stresses, and surface temperature in the prognostic mode. Therefore, the prognostic mode will use the LGM background boundary conditions instead of PD to calculate the wind anomalies. The simulated CAM winds are 33% and 50% stronger than the UVic winds in the Southern and Northern Hemispheres, respectively (Figure S1a). Since the dynamical wind feedback option from UVic is turned on, winds are allowed to change during all the experiments. Consequently, atmospheric moisture advection terms and turbulent surface heat forcing are calculated consistently by the model without flux correction.

To further explore the role of the wind stress on the stability of the AMOC, we performed two additional simulations in which the winds are only strengthened in one of the hemispheres. In these simulations, only the standard vertical mixing coefficient ($A = 0.8 \text{ cm}^2/\text{s}$; described in the next section) is implemented. This is shown in Figure 1 as the magenta and light blue lines, for strengthened Northern Hemisphere (NHCAMA0.8) and Southern Hemisphere (SHCAMA0.8), respectively. Each experiment is run with and without freshwater hosing, as described in section 2.4.

2.3. Vertical Mixing

To understand the sensitivity of the AMOC stability to the strength of the mean wind and of the AMOC, we produce two ensembles, one for each wind forcing, in which varying vertical mixing strength is applied via parameter change. Vertical mixing is responsible for bringing water back to the surface and for increasing the potential energy against stratification in the Earth system, which is heated at the surface. Without it, the circulation would collapse due to the strong vertical stratification. Indeed, previous studies show that vertical mixing parameters are highly uncertain in low-resolution models, since they are calibrated to

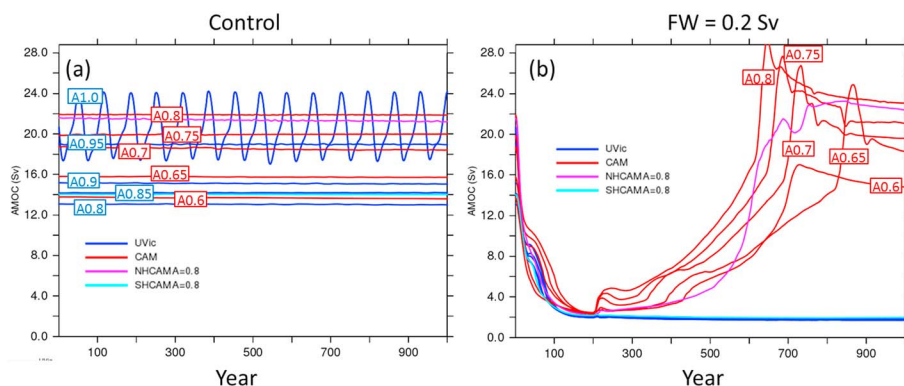


Figure 1. AMOC strength (Sv) of the two ensembles with varying vertical mixing parameter for UVic winds (blue), CAM winds (red), and CAM winds in the Northern Hemisphere (magenta) and in the Southern Hemisphere (light blue). Panel (a) is for Last Glacial Maximum CONTROL and (b) is for the hosing experiments using FW = 0.2Sv during the first 200 years. The values of the mixing parameters are displayed in the boxes. AMOC = Atlantic Meridional Overturning Circulation; UVic = University of Victoria.

represent several mixing sources that are not present in those models (e.g., Goes et al., 2010; Ito & Marshall, 2008). Under the Brian and Lewis parameterization, vertical mixing (K_v) varies with depth according to the following equation:

$$K_v = A + \frac{B}{\pi} \arctan(\gamma(z-z_0))$$

where $z_0 = 2500$ m is the depth of inversion, $B = 1.05$ is a scale, and A is an offset. The most effective way to vary K_v is to change the parameter A , which acts as an offset for the whole water column. We vary parameter A within approximately 25% from its default value of $0.8 \text{ cm}^2/\text{s}$, reducing to $A = [0.6, 0.65, 0.7, 0.75, 0.8] \text{ cm}^2/\text{s}$ in the CAM wind simulations, and increasing to $A = [0.8, 0.85, 0.9, 0.95, 1.0] \text{ cm}^2/\text{s}$ in the UVic simulations (Figure S1b).

We adopt a standard nomenclature for the ensemble runs (see Table S1) to represent both wind and vertical mixing uncertainty, the UVic wind ensemble (UVicA), the CAM wind ensemble (CAMA), the Southern Hemisphere (SHCAMA), and Northern Hemisphere (NHCAMA) CAM wind forcing, and include as a suffix the value of the parameter A to identify each individual run. Therefore, our simulations that use the standard mixing of $A = 0.8 \text{ cm}^2/\text{s}$ are referred to as UVICAO.8, CAMAO.8, SHCAMA0.8 and NHCAMA0.8.

2.4. Freshwater Forcing and AMOC Stability

Changes in the mean wind state have strong implications on the stability of the AMOC. Using a freshwater budget in the Atlantic Ocean north of 34°S , Murphy et al. (2017) presented a stable AMOC behavior under CAM winds in three different freshwater hosing experiments varying from $\text{FW} = 0.1$ to 0.3 Sv . In these simulations the AMOC recovered to its original state following 200 years of hosing. Under weaker UVic winds, the AMOC collapsed in all simulations that used $\text{FW} > 0.03 \text{ Sv}$, a tipping point reached with much less freshwater applied in the Northern Hemisphere compared to the CAM winds experiments. Those results suggested that the recovery of the AMOC was related to the sign of the meridional overturning freshwater transport (M_{ov}) across the southern boundary (34°S), and potentially associated with the mean state of the AMOC, which was much stronger under CAM winds forcing. Since those simulations featured very different mean states of the AMOC, here we analyze the instability of the AMOC using the expanded ensembles that share similar AMOC strengths but different wind forcing. We apply the same magnitude of freshwater hosing ($\text{FW} = 0.2 \text{ Sv}$) in the North Atlantic between 45°N and 65°N (Figure 1b) for 200 years, after which it is turned off.

Additional freshwater simulations were performed under a quasi-steady state. These simulations are run for 5,000 years, in which the freshwater forcing varies from 0 to 0.2 Sv (years 0–2000), then from 0.2 Sv back to 0 Sv (years 2,000–4,000) at a rate of $1 \times 10^{-3} \text{ Sv/year}$ and kept at 0 Sv for additional 1,000 years. Hysteresis curves can be drawn from these simulations.

3. Results and Discussion

The mean state of the AMOC strength using the same vertical mixing parameter ($A = 0.8$) but subject to different wind forcing is very different as discussed in section 2.2. The westerlies in the UVicA0.8 simulation are weaker than the PD climatology (Figure S1a), and the mean AMOC strength is around 13 Sv. Conversely, in the CAMA0.8 simulation the westerly winds are stronger than the PD climatology and displaced further south in the Southern Hemisphere (Figure S2), which produces a stronger AMOC of 22 Sv. The AMOC strength is also proportional to the vertical mixing parameter A , and for higher values of A the AMOC is stronger. Therefore, in both wind ensembles with varying vertical mixing strength, the AMOC shares the same range of mean states from 13 to 22 Sv (Figure 1a). Interestingly, the simulation under UVic winds and large mixing (UVicA1.0) produces spontaneous multidecadal variability with amplitude of approximately 6 Sv. This multidecadal variability is associated with a dipole structure in the upper ocean (500 m) temperature and salinity between the Gulf Stream region and the subpolar gyre (Figure S3), similar to what is described in Zhang (2008) and Delworth and Mann (2000). The anomalous temperature pattern is associated with a similar salinity pattern of the same phase. In the subpolar gyre, the evolution of this pattern follows a westward propagation, consistent with the thermal Rossby wave propagation timescales described in Te Raa and Dijkstra (2003). Vertical mixing in this case acts as the damping of a delayed oscillator.

The AMOC stream function in depth coordinates (Figure S4) between the simulations in each ensemble with similar AMOC strengths, that is, for strong AMOC (~22 Sv, UVicA1.0 vs. CAMA0.6) and weak AMOC (~13 Sv, UVicA0.8 vs. CAMA0.6) are very similar. The depth of the upper cells are nearly identical between the pair of simulations, which is deeper (~3,000 m) for the strong AMOC simulations, and shallower (~2,200 to 2,400 m) for the weak AMOC simulations. Different patterns emerge (Figure 2) when we compare the AMOC stream functions in density (σ_2) coordinates. The CAMA simulations (Figures 2a and 2c) have generally a denser upper cell relative to their UVicA counterparts (Figures 2b and 2d), with the σ_2 density of the North Atlantic Deep Water (NADW) ranging between 37.0 and 37.4 kg/m³, compared to the UVicA runs in which the NADW ranges from 36.9 to 37.2 kg/m³. In addition, the NADW under CAMA spreads further south than in the UVicA for similar AMOC strengths. This is expected, since for the same AMOC strength UVicA runs are subjected to stronger and more effective vertical mixing, due to their reduced middepth ocean stratification. The integrated isopycnal transport in the Atlantic domain of the Southern Ocean (note that it is not defined as a stream function) shows that there is more vigorous Southern Ocean upwelling, more Antarctic Intermediate Water (AAIW) formation, and denser Antarctic Bottom Water (AABW) under the stronger winds in CAMA. The average AABW formation in the Atlantic is about 50–60 Sv in both ensembles, of which only about 2–4 Sv spreads into the Atlantic basin; the rest upwells in the Indo-Pacific basin. Studies based on PD observations estimate that between 3 to 6 Sv of AABW is transported across 32°S in the Atlantic ocean (e.g., Lumpkin & Speer, 2007; Talley, 2013). These AABW transports are similar to the estimates for the LGM from models (Jansen, 2017). Observational estimates of the AABW formation around Antarctica are not well constrained, with some estimates ranging from 21–50 Sv (e.g., Sloyan & Rintoul, 2001; Lumpkin & Speer, 2007; Talley, 2013). Lee et al. (2019), using the National Center for Atmospheric Research CESM1 model constrained to observed temperature and salinity climatologies, estimated that more than 35 Sv of AABW is formed near Antarctica in the PD, but only a small amount of bottom water is transported north of 32°S in the Atlantic, such that most of the AABW either spreads to the Indo-Pacific basins or recirculates back to the surface. Although there are deep uncertainties in the observational and model estimates of the AABW formation, UVic estimates presented here certainly overestimate the AABW formation and recirculation in the Southern Ocean, which is a region of important interactions with topography.

The stronger stratification under CAMA for comparable AMOC strengths can be set by the location of the NADW formation region in the subpolar North Atlantic (Figure 3). The maximum winter mixed layer depth is similar under the two wind ensembles, with a maximum of approximately 500–550 m, and it is wider and deeper when the AMOC is stronger. In CAMA, the NADW formation is more strongly mechanically driven. The ice edge is displaced north of 60°N, which is the effect of an approximately ~25% stronger northward heat transport in CAMA. The ice edge affects the location of the convection region, and for CAMA more deep-water is formed south of Greenland and the Irminger Sea instead of near the British Isles. Note that in the PI simulation, the location of the deep convection in the subpolar North Atlantic is typically mostly located near the British Isles, instead of the Labrador and Greenland-Iceland-Norwegian seas. However,

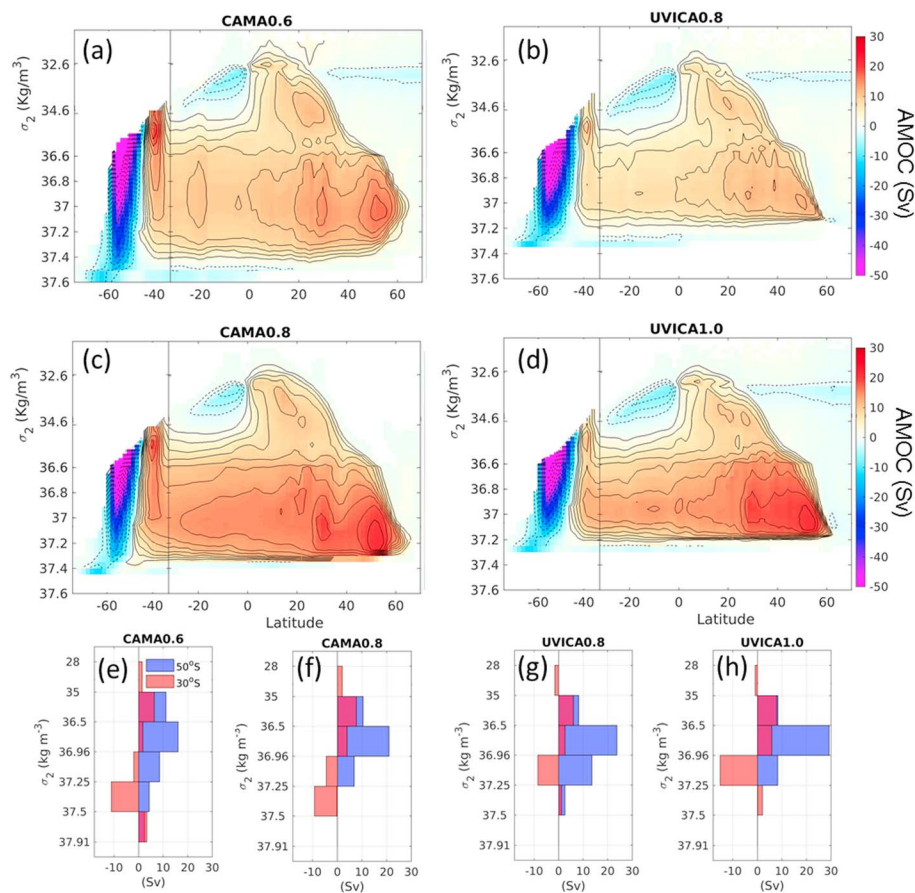


Figure 2. (a–d) AMOC stream function (Sv) in density coordinates for the Last Glacial Maximum CONTROL simulations. Density is calculated relative to 2,000 m (σ_2 , kg/m³). Note that this only takes into account the Atlantic sector; thus, the Southern Ocean (south of 34°S) does not represent a stream function. Top panels are for weak AMOC under two different wind forcings (a) CAMA0.6 and (b) UVicA0.8, and middle panels are for strong AMOC (c) CAMA0.8 and (d) UVicA1.0. Bottom panels (e–h) are the respective volume transports calculated in 6 isopycnal ranges and two latitudes, 50°S (purple) and 30°S (orange). AMOC = Atlantic Meridional Overturning Circulation; UVic = University of Victoria.

the location of deepwater formation south of Greenland in LGM simulations is similar to more sophisticated coupled climate models (Otto-Bliesner & Brady, 2010; Sherriff-Tadano et al., 2018).

3.1. Stability of the AMOC Under Wind and Vertical Mixing Uncertainty

Here we analyze the AMOC stability under a constant freshwater forcing scenario (FW = 0.2 Sv). Perhaps surprisingly, the AMOC still shows a bipolar behavior, with the ones under UVicA winds collapsing and the ones under CAMA winds returning to its original strength (Figure 1b). Therefore, it is the wind forcing rather than the strength of the AMOC/vertical mixing that determines the stability of the AMOC in these simulations. It is important to mention that this result is valid for the set of parameters and the range of parameter values analyzed in the present study, and alternative methods may produce different results. Our results are not dependent on the strength of freshwater input, since in quasi-steady state incremental freshwater hosing experiments of 5,000 years (Figure S5), CAMA is monostable and UVicA is bistable in both high and low mixing cases when the freshwater forcing is ceased. This is in contrast with previous studies that analyzed simulations with similar AMOC ranges (e.g., Gregory et al., 2005; Sijp & England, 2006) that suggested that the AMOC stability could be associated with the vertical mixing parameterization and the mean state of the AMOC. In the CAMA simulations with a stronger mean AMOC ($A = 0.7, 0.75$, and 0.8) the AMOC overshoots during the recovery (Figure 1b), but this behavior is much attenuated for the simulation with a weak AMOC (CAMA0.6).

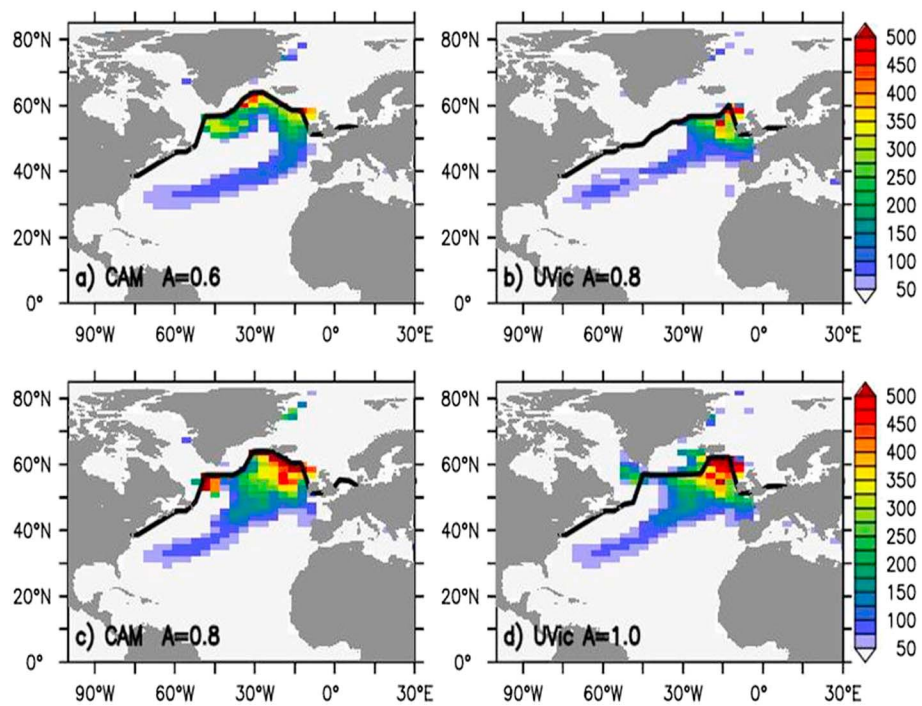


Figure 3. Ventilation depth (m) for the Last Glacial Maximum CONTROL simulations with weak AMOC (a) CAMA0.6 and (b) UVicA0.8, and simulations with strong AMOC (c) CAMA0.8 and (d) UVicA1.0. The black lines represent the ice edge in those simulations. AMOC = Atlantic Meridional Overturning Circulation; UVic = University of Victoria.

We analyze the ocean freshwater transport (OFTW) terms of the freshwater budget in the Atlantic Ocean in the two ensembles (Figure 4). In a steady state (control) simulation, OFWT at any given latitude (φ) is approximately equal to the net evaporation (ENET) integrated north of φ : $ENET \approx OFWT = Mov + Maz$, where OFWT can be divided into meridional overturning (Mov) and gyre (Maz) freshwater transports (De Vries & Weber, 2005). The Bering Strait is closed in all simulations, so the freshwater transport terms at 34°S can be also interpreted as freshwater convergence terms in the Atlantic basin (Liu, Liu, Cheng, & Hu, 2014).

Despite the large range in AMOC strength, the freshwater budget terms in each ensemble do not significantly change as indicated by the width of the uncertainty envelopes in Figures 4a and 4b. Some spread is observed in the Mov and Maz terms, which compensate each other, such that ENET is insensitive to the vertical mixing uncertainty. At 34°S, the CAMA ensemble shows stronger net evaporation, 220 mSv (1 mSv = $1e^3$ m³/s) compared to 170 mSv for the UVicA ensemble, showing that the stronger winds increase evaporative cooling in the Atlantic Ocean. At 34°S, the ENET in the CAMA ensemble is compensated almost equally by both Mov and Maz terms, which are both positive. In the UVicA ensemble (Figure 4a), ENET is compensated mostly by a positive Maz, and the magnitude of Mov is much smaller, less than 25% of ENET. To note, Mov is not strictly negative in all UVicA simulations, and its value can reach 43 mSv for the simulations with high vertical mixing (UVicA1.0). Therefore its sign cannot be considered as the only measure of stability. Weber et al. (2007) noticed that PMIP2 models that present an unstable AMOC could indeed have both signs of Mov, but that they were all smaller than the other freshwater terms, indicating they were close to a bifurcation point. Thus, our results are not in disagreement with previous studies. The model still behaves according to the salt advection feedback (Figures 4c and 4d), in which in the stable AMOC simulations (CAMA), the AMOC weakens after the end of the external freshwater input in the North Atlantic, and its related freshwater transport moves from importing to exporting freshwater away from the Atlantic (Mov in Figure 4d). Alternatively, in the unstable AMOC simulations (UVicA), the weakened AMOC increases the import of freshwater into the Atlantic (Mov in Figure 4c). There are differences in the initial rate of the Mov changes in CAMA and UVicA during the 200-year hosing forcing period. In UVicA, the Mov responds almost instantly to the forcing, whereas in CAMA there is an initial increase of the Mov before changing sign.

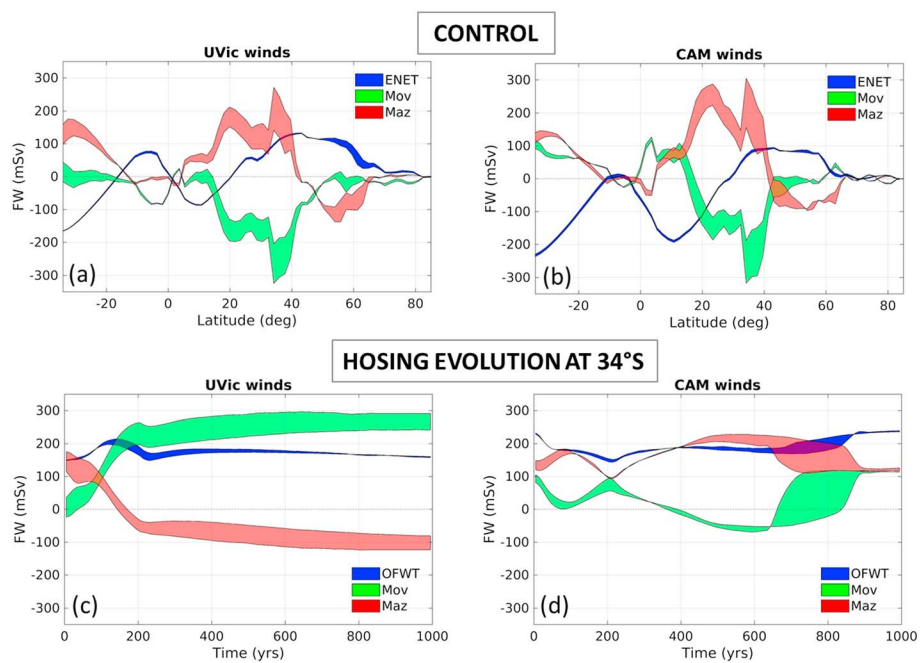


Figure 4. Freshwater budget terms calculated for the envelope of the whole ensemble range. Top panels are for the variability with latitude in the Last Glacial Maximum CONTROL simulation and lower panels are the time evolution of the terms at 34°S during the 1,000 years of simulation with hosing applied during the first 200 years. (a, c) UVicA ensemble and (b, d) CAMA ensemble. UVic = University of Victoria; ENET = net evaporation; OFWT = ocean freshwater transport.

This can be explained by temperature feedbacks and by the amount of freshwater that is required for the CAMA to collapse, which is about 10 times more than in UVicA, since the latter is close to a point of collapse (Murphy et al., 2017).

Here we explore the role of wind stress on the stability of the AMOC in the NHCAMA0.8 and SHCAMA0.8 experiments. The mean AMOC strength for the simulation with stronger NH winds (NHCAMA0.8) shows that the NH winds can maintain a strong AMOC of ~22 Sv, a similar result to the one found in Muglia and Schmittner (2015). When freshwater hosing is applied to this simulation (Figure 1b), the AMOC recovers, similar to the other CAMA experiments, but with a slower initial recovery compared to the other CAMA simulations (Figure 1b). After 500 years (300 years after hosing termination) the rate of AMOC recovery strengthens considerably, matching the one with CAMA0.8, but the overshoot before stabilization was much reduced. By changing only the SH winds (SHCAMA0.8), however, the mean AMOC strength is much weaker (14 Sv), and the AMOC does not recover after the hosing termination. This suggests that stronger NH winds controls the stability of the AMOC, not stronger SH winds. Stronger SH winds can, however, accelerate its recovery. Previous studies that used coarse-resolution ocean models suggested that the AMOC is significantly more vigorous under stronger SH winds in models (e.g., Gnanadesikan, 1999; Saenko, 2013; Toggweiler & Samuels, 1993). This is theorized to be due to what is called the “Drake Passage effect,” where in the absence of continental barriers in the Southern Ocean westerly winds create a northward Ekman transport in the Atlantic that cannot be balanced by geostrophic transport and is mostly balanced by an increase in the NH AMOC. More recently (see Gent, 2016, for a review), eddy resolving model experiments show that eddy transport increases in response to increased Ekman transport from the SH winds, providing an average of 50% of a transient eddy-overturning compensation to the strengthened Southern Ocean AMOC cell, and most of this increase remains in the south. Gent and Danabasoglu (2011) showed improvements in the model eddy compensation using a variable GM coefficient in space and time. Here we use a somewhat increased GM coefficient ($800 \text{ m}^2/\text{s}$) and surface boundary conditions that may allow some degree of compensation; therefore, the AMOC strength is not very sensitive to the wind increase in the SH. It is still largely unclear how the SH westerly winds changed during the LGM, although a strengthening and

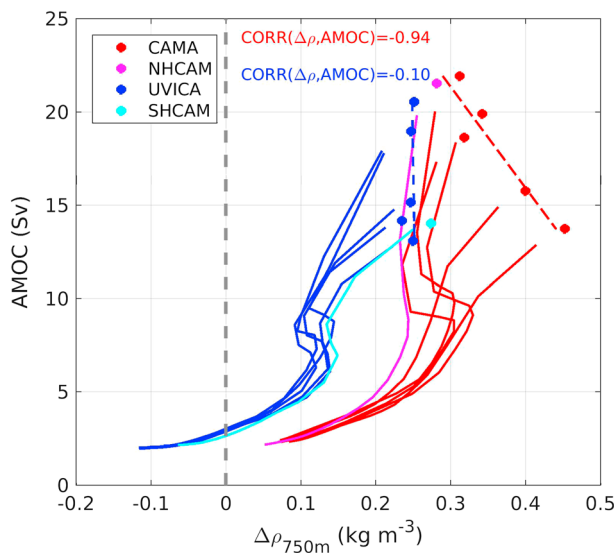


Figure 5. Relationship between AMOC and meridional density differences relative to 2,000 m ($\Delta\rho$) averaged between two regions ($45\text{--}55^\circ\text{N}$) and ($40\text{--}35^\circ\text{S}$) at the nominal depth of 750 m. Dots are for the Last Glacial Maximum CONTROL simulations and lines are for the evolution of the initial 200 years of the freshwater hosing experiments. Colors are for CAMA (red), NHCAMA0.8 (magenta), SHCAMA0.8 (light blue), and UVICa (blue) simulations. Gray dashed line shows the zero crossing of density differences. Colored dashed lines indicate the linear regression between $\Delta\rho$ and AMOC on their respective control LGM simulations (UVICa, blue dashed line and CAMA, red dashed line), and their respective correlation coefficients are also shown. AMOC = Atlantic Meridional Overturning Circulation.

poleward shift shows the best agreement with a SH moisture database (Kohfeld et al., 2013; Sime et al., 2013).

As shown in Figure 2, the density of the AMOC and water column stratification is significantly different between the two wind ensembles. Previous studies using box model arguments indicate that the pressure difference between the North and South Atlantic is proportional to the strength of the AMOC (Rahmstorf, 1996; Stommel, 1961). The pressure difference can be approximated by the density difference ($\Delta\rho$) at fixed latitudes averaged at the pycnocline depth (Wright & Stocker, 1991). Here, we follow Rahmstorf (1996) and define this AMOC indicator as the density difference relative to 2,000 m (σ_2) between the North (50°N to 55°N) and South (35°S to 40°S) Atlantic averaged at middepth between 650 and 850 m (nominal of 750 m). In the CAMA ensemble (Figure 5), the control simulations (red dots) have a quasi-linear relationship between the mean AMOC strength and $\Delta\rho$, showing a correlation of -0.94 . The linear relationship is in agreement with the thermal wind relationship, in that the density gradients are proportional to the velocity shear. The slope is negative, since it is mostly driven by salinity differences in the LGM, which is not the case for present-day simulations (see Figure 10 in de Boer et al., 2010) because of the nonlinearity of the equation of state. This linear relationship is not found in the UVICa simulations (blue dots), for which the pressure difference is practically unresponsive to vertical mixing changes and correlation between AMOC and $\Delta\rho$ is -0.1 . This difference must be due to the differences in vertical stratification between the two ensembles, and in UVICa, the meridional density gradients may not contribute directly to pressure differences (de Boer et al., 2010). The evolution diagram for the hosing experiments in the first 200 years of simulation (solid lines) shows a

relationship between the AMOC strength and $\Delta\rho^{1/3}$ in both ensembles, as observed by the S-shaped curves in Figure 5. Therefore, both ensembles agree with the assumption of an upwelling-diffusion balance and the independence of the AMOC flow rate to the depth scale (e.g., de Boer et al., 2010; Welander, 1986). The behavior of the NHCAM and SHCAM agree with their respective ensemble behavior (CAMA and UVICa) described in Figure 1b. The UVICa simulations show a change in sign of the pressure gradient when the AMOC goes below 3 Sv, and the north-south density gradient can no longer sustain the AMOC, thus the AMOC collapses. Therefore, $\Delta\rho$ can be used as an indicator for the AMOC recovery from collapse in the present simulations. The use of this indicator to identify the stability of the AMOC from the initial value in the LGM control simulation is still to be examined.

The stronger stratification under CAMA winds impacts the distribution of water masses across the Atlantic basin. This is shown in the salinity and temperature differences between the control simulations in UVICa and CAMA (Figure 6). The average of all simulations contained in each wind forcing is shown, so the results are not dependent on the AMOC strength. The sea surface salinity in the CAMA winds is generally higher in the northern subpolar gyre where winds are stronger. In addition, there is increased evaporation, and increased salinity transport northward from the salty tropics under a stronger and less diffusive Gulf Stream current flowing along the western boundary. South of 40°N , however, the CAMA ensemble shows a broad freshening of the basin relative to the UVICa ensemble. Since the evaporation is stronger in CAMA compared to UVICa, this freshening cannot be driven by atmospheric E-P fluxes, as diagnosed by Liu, Liu, Cheng, and Hu (2014). The zonal average section of salinity in the Atlantic suggests that there is a stronger tongue of fresh AAIW under CAMA winds (Fig. 6e), which is consistent with previous studies in which stronger westerlies strengthen the formation of AAIW via Ekman divergence. The mismatch is then explained by the increased upwelling of these fresher AAIW waters in the tropics. This is also corroborated by weaker stratification in the UVICa simulations, so less energy is necessary to pull the AAIW waters to the surface. The increased stratification in the CAMA ensemble, shown by the tighter isopycnal range is driven by the stronger winds. This causes a cooling of the basin (Fig. 6i), and an increase in the salinity at

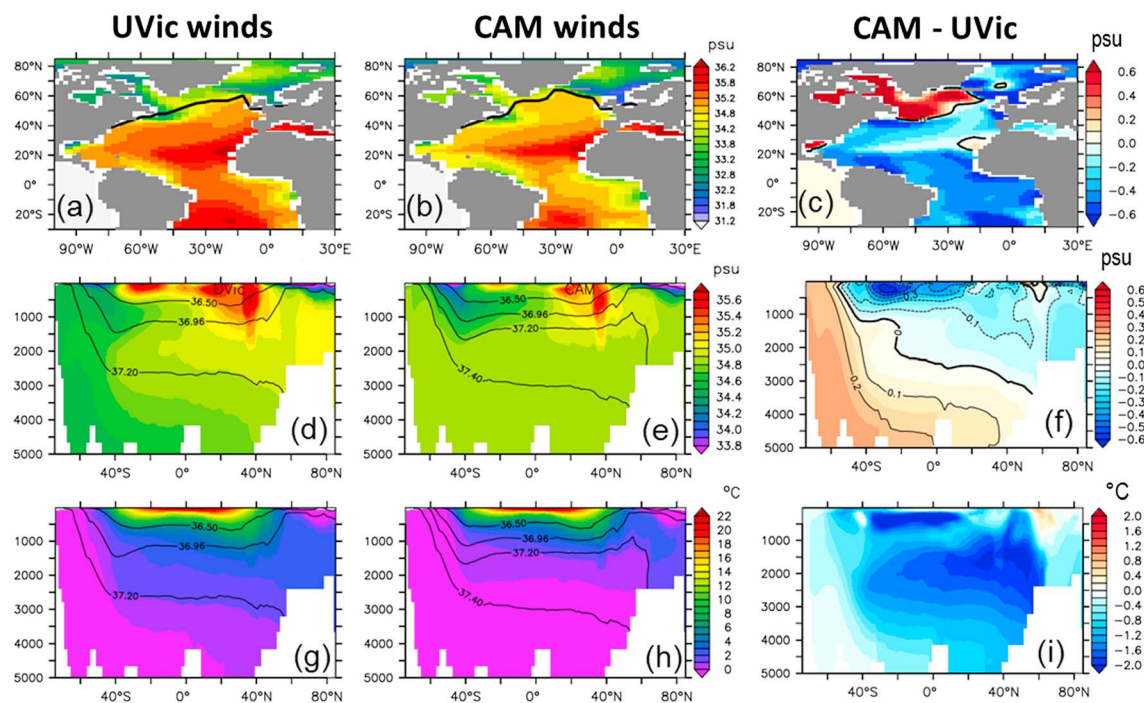


Figure 6. Last Glacial Maximum sea surface salinity (top row), zonal averaged sections of salinity (middle row), and temperature (bottom row) across the Atlantic Ocean. Panels are averages of all (a, d, and g) UVicA simulations, (b, e, and h) CAMA simulations, and (c, f, and i) CAMA-UVicA. The ice edge is drawn in panels (a) and (b), and the σ_2 surfaces are drawn in section panels (d, e, g, and h). UVic = University of Victoria.

depth (Figure 6f), since below 2,000 m the water column is mostly occupied by the AABW, which is saltier due to brine rejection around Antarctica (Amrhein et al., 2018). The vertical structure of the salinity differences (CAM-UVic), with freshening at the surface and salinification underneath induces the increased northward freshwater transport across 34°S (Figure 4b).

3.2. Comparison With Proxy Data

In a recent study, Amrhein et al. (2018) used sea surface temperature (SST) proxy data to calibrate the ocean circulation in an LGM simulation using an adjoint model framework. This is important since there are no direct ocean hydrography profile measurements available for the LGM. The impact of surface temperature data on inferences of abyssal properties would then be mediated by correcting deep-water formation processes, which are highly parameterized in low-resolution models. In addition, SST is shown to be the major driver of LGM wind changes in the Southern Ocean (Sime et al., 2013). Here, we compare the mean LGM state under the two wind forcings to the reconstruction by Annan and Hargreaves (2013), which calculates the LGM SST difference relative to the PI (Δ SST) using a blend of PMIP2 model simulations and proxy data. For our model simulations, the baseline PI simulation is a control UVic simulation with boundary conditions from year 1,800 (atmospheric CO₂ ~284 ppmV), which uses the tidal mixing parameterization for vertical mixing to increase mixing over topography, and a background mixing of $K_{bg} = 0.25 \text{ cm}^2/\text{s}$, as described in Goes et al. (2014). The maps of Δ SST anomalies (LGM-PI) compared to the paleo Δ SST reconstruction are shown in Figure 7. There is a positive bias in the Southern Ocean in the UVicA experiments of up to 3 °C in some locations, which is slightly reduced in the CAMA experiments. This result suggests that SST biases are reduced relative to the reconstruction when there is strong evaporative cooling due to stronger winds, which acts to reduce the meridional SST gradient with the subtropics. In the subpolar North Atlantic, all simulations show a positive SST bias of more than 2 °C in the center east part of the gyre, which can be partly attributed to the wrong location of the convection zone in the UVic PI experiment. These positive biases are enhanced for stronger AMOC simulations (Figures 7c and 7d). The errors are the smallest in the tropical Atlantic (<1 °C), whereas the tropical Indo-Pacific regions are generally cooler in the LGM simulations

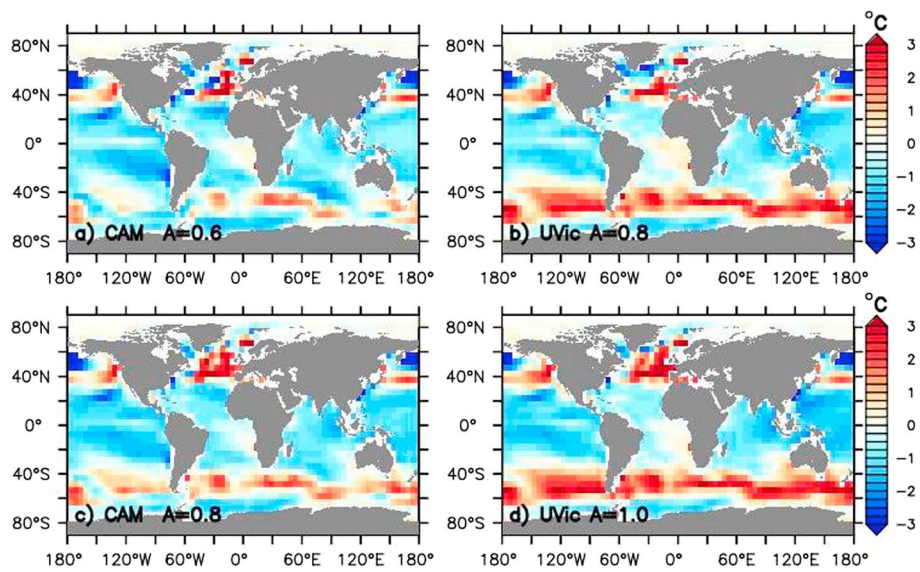


Figure 7. Biases in SST changes (LGM-PI) relative to the Annan and Hargreaves (2013) reconstruction using proxy data and Paleoclimate Model Intercomparison Project Phase 2 model simulations. Panels (a) and (c) are for the CAMA simulations with parameter $A = 0.6$ and $A = 0.8$, respectively, and panels (b) and (d) are for the UVicA simulations with parameter $A = 0.8$ and $A = 1.0$, respectively. The PI UVic simulation used to calculate LGM-PI SST change was used in Goes et al., (2014). LGM = Last Glacial Maximum; PI = Preindustrial; SST = sea surface temperature.

than estimated by the proxy data. To infer which of the two simulated ensemble uncertainties brings the best match with the ΔSST proxy data, we use an analysis of variance methodology. This methodology is appropriate for comparing means of different experiments, and the marginal error distributions for individual parameters can be easily retrieved. In a nutshell, this is performed by decomposing the absolute values of SST biases from Figure 7 into Kv and wind components:

$$y \sim \mu + a[i] + b[j] + \epsilon$$

where μ is the baseline error common to all simulations, the parameter $a[i]$, $i = 1:5$ is related to the five Kv values and $b[j]$, $j = 1:2$ is related to the two background wind strengths, and ϵ is the residual error, which is assumed to be normally distributed with zero mean. The corner constraint is imposed, where $a[1], b[1] = 0$, and the other parameters are estimated using a Bayesian framework following the methodology of Goes et al. (2017).

According to the analysis of variance results (Figures 8a and 8b), the magnitude of ΔSST biases in the UVicA simulations is higher than in the CAMA for all ensemble members. In the base case (UVicA, $Kv1$), the global ocean ΔSST bias is $\sim 1^\circ\text{C}$, in comparison to $\sim 0.85^\circ\text{C}$ for the CAMA (Figure 8a), and the mean relative bias in the CAMA ensemble is approximately 0.12°C smaller than in UVicA (Figure 8e). By decomposing the error relative to the $Kv1$ baseline, we can observe that the magnitude of the bias due to Kv increases with increasing Kv (Figure 8c). The marginal errors due to Kv uncertainty are small ($<0.08^\circ\text{C}$) but statistically significant compared to $1-\sigma$ standard error bars (Figure 8c). The same conclusions can be drawn when the method is applied to the Southern Ocean ($40\text{--}60^\circ\text{S}$) only (Figures 8b, 8d, and 8f), with similar differences due to Kv but stronger reduction of the bias ($\sim 0.55^\circ\text{C}$) in CAMA ensemble (Figure 8f) relative to UVicA.

Therefore, our results indicate that there was a slightly weaker AMOC in the LGM (13 Sv) compared to the UVic PI (16 Sv) but that there also was a stronger mechanically driven AMOC in the Northern Hemisphere. Even though SST proxies are a weak constraint for the LGM climate as stated by Muglia and Schmittner (2015), these results are quantitatively similar in that stronger Northern Hemisphere winds can sustain the AMOC under lower vertical mixing, and a shallower AMOC is more consistent with isotope paleo proxies (Muglia et al., 2018).

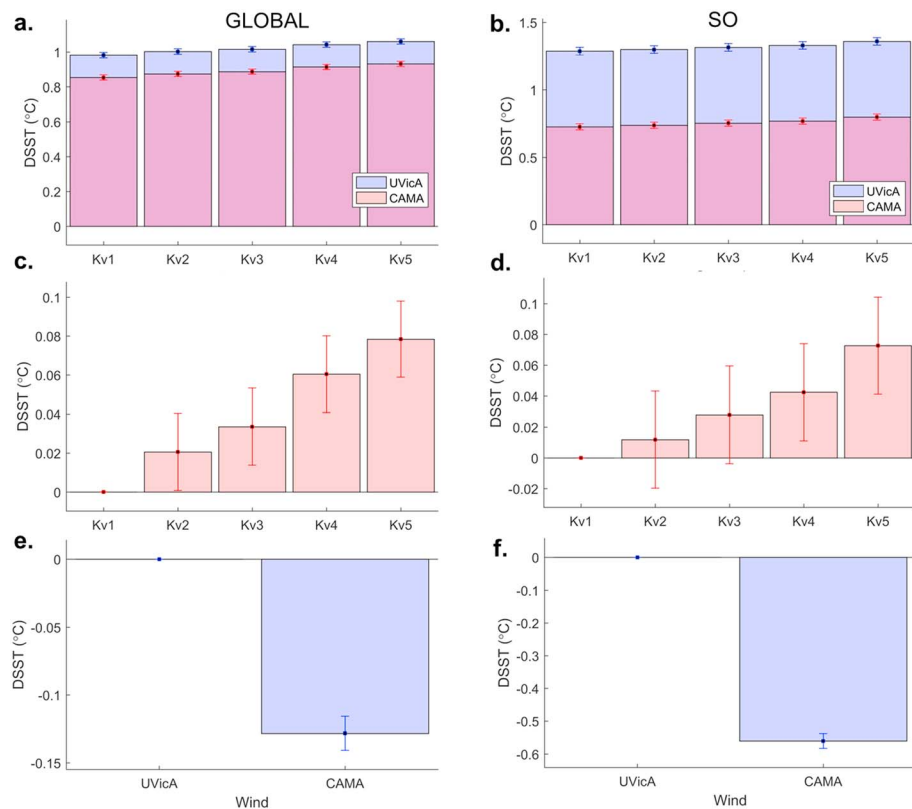


Figure 8. Analysis of variance method of ΔSST (Last Glacial Maximum-Preindustrial) biases relative to the proxy reconstruction of Annan and Hargreaves (2013). Statistics are shown for global (left column) and Southern Ocean (right column) estimates. (a, b) Total biases for each ensemble simulation, blue bars for UVicA, and red bars for CAMA simulations. (c, d) Contributions to biases from vertical mixing relative to the low K_v baseline (K_v1). (e, f) Contributions to biases from wind strength relative to UVicA baseline. SST = sea surface temperature.

4. Conclusions

In this paper, the stability of the AMOC under LGM/HS1 boundary condition is tested in two ensembles varying the (i) mean wind forcing and (ii) the background vertical mixing. The AMOC strength is very sensitive to these two parameters, and the AMOC strength in each of the two wind forcings (e.g., UVicA and CAMA) control ensembles ranges from 13 to 22 Sv. HS1 events were simulated using a freshwater input of 0.2 Sv in the North Atlantic for 200 years. Contrary to what has been suggested in previous studies, the mean state of the AMOC strength (via vertical mixing parameter changes) was not associated with its stability. Instead, in the two ensembles analyzed, the strength of the Northern Hemisphere winds was the single factor determining the AMOC recovery due to its stronger impact on the water column stratification and the density of the NADW formation.

The most commonly used AMOC stability indicator, the sign of the Mov at 34°S, was not an absolute measure for stability, since the high mixing/weaker winds (UVicA0.95, 1.0) simulations showed a weakly positive Mov (30–50 mSv) associated with a strong (~22 Sv) but unstable AMOC. After hosing termination, both stable (CAMA) and unstable (UVicA) ensembles behave similar to a salt advection feedback, in which for the un (stable) simulations, the weakened AMOC increases (decreases) the import of freshwater into the basin, providing a positive (negative) feedback to further decrease (increase) the AMOC. Therefore, this mechanism partially explains the AMOC stability in these ensembles. From scaling arguments, the AMOC strength has been associated with the meridional density difference between the north and south ($\Delta\rho$) across the Atlantic basin (e.g., Welander, 1986). A linear relationship is found between the mean AMOC strength and the density gradient in the control CAM wind ensemble, but this relationship was not significant under weaker UVicA simulations. A stronger AMOC- Δ relationship, such as the one

shown in the CAMA ensemble, represents a more adiabatic AMOC, where NADW upwelling occurs mostly in the Southern Ocean instead of in the tropics. Under freshwater hosing, the AMOC behavior in both ensembles appears to be proportional to $\Delta\rho^{1/3}$, which according to previous studies, this relationship satisfies a diffusive depth scale given by the thermal wind equation (Bryan, 1987). In all simulations that showed a bistable AMOC behavior, the sign of $\Delta\rho$ becomes negative after the hosing termination, and, therefore, the density gradient cannot sustain the AMOC.

We eliminate the effect of vertical mixing by averaging over all simulations in each wind ensemble to examine the impact of wind forcing on Atlantic Ocean water masses. Since both ensembles share the same range of AMOC strength, the differences in water masses are driven solely by the strength of the wind forcing. Stronger winds (CAMA) increase the middepth ocean stratification, causing a more sluggish abyssal ocean. The volume of the AABW increases under stronger wind forcing, and its high salinity signal is detected much further north in the North Atlantic. These features have been suggested for LGM mean climate (Muglia & Schmittner, 2015; Wainer et al., 2012). In addition, the AAIW is both increased and shallower, and upwells more strongly in the tropical basin, freshening the surface. As a consequence, sea surface salinity decreases in most of the Atlantic basin, with the exception of the subpolar North Atlantic where a large increase in salinity promotes a stronger and denser AMOC.

Paleoclimatic records are inconsistent on the strength of the LGM AMOC but tend to point toward a shallower North Atlantic cell. In studies that indicate a weaker cell, the decreased NADW formation is accompanied by increased intrusion of the AABW into the Atlantic basin (Curry & Oppo, 2005; Sarnthein et al., 1994). Models, similarly, diverge about the mean AMOC response to LGM boundary conditions (Brady et al., 2013). Comparing our simulations with a global ΔSST (LGM-PI) reconstruction, the simulation that shows the lowest errors is the one with increased westerly winds and the lowest vertical mixing (CAMA0.6). Features in this simulation agree with recent paleomodeling studies (e.g., Muglia et al., 2018) that show a weaker AMOC strength (~13 Sv), and increased AABW volume in the Atlantic Ocean during the LGM. According to our results, the AMOC was in a stable state, which still can sustain an off-state, although not spontaneously, only under freshwater forcing conditions (HS1). Our results may be dependent on the background climate state (Zhu et al., 2014), regional features such as sea ice extent and ice sheets (Klockmann et al., 2016; Zhang, 2014), the opening of the Bering Strait (Hu et al., 2015), and mixing parameters considered, which includes eddy mixing parameterization (Gent, 2016) uncertainty.

Acknowledgments

M. Goes was supported by NOAA's Climate Program Office (Climate Variability and Predictability Program Award GC16-207), the National Science Foundation (NSF-1537769), NOAA/AOML, and University of Miami/CIMAS under the cooperative Agreement NA15OAR4320064. L.N. Murphy and A.C. Clement were supported by the National Science Foundation Grant NSF-1735245. The authors thank Peter Gent and an anonymous reviewer for their comments that greatly improved the final version of the paper, and the USAMOC Task Team 3 and Task Team 5 for comments and suggestions. Model simulations will be made available under scholarlyrepository.miami.edu/ website.

References

- Amrhein, D. E., Wunsch, C., Marchal, O., & Forget, G. (2018). A global glacial ocean state estimate constrained by upper-ocean temperature proxies. *Journal of Climate*, 31(19), 8059–8079. <https://doi.org/10.1175/JCLI-D-17-0769.1>
- Annan, J. D., & Hargreaves, J. C. (2013). A new global reconstruction of temperature changes at the Last Glacial Maximum. *Climate of the Past*, 9(1), 367–376. <https://doi.org/10.5194/cp-9-367-2013>
- Barker, S., Chen, J., Gong, X., Jonkers, L., Knorr, G., & Thornalley, D. (2015). Icebergs not the trigger for North Atlantic cold events. *Nature*, 520(7547), 333–336. <https://doi.org/10.1038/nature14330>
- Bitz, C. M., Holland, M. M., Weaver, A. J., & Eby, M. (2001). Simulating the ice-thickness distribution in a coupled climate model. *Journal of Geophysical Research*, 106(C2), 2441–2463. <https://doi.org/10.1029/1999JC000113>
- Böhm, E., Lippold, J., Gutjahr, M., Frank, M., Blaser, P., Antz, B., et al. (2015). Strong and deep Atlantic meridional overturning circulation during the last glacial cycle. *Nature*, 517, 73–76. <https://doi.org/10.1038/nature14059>
- Braconnot, P., Otto-Bliesner, B., Harrison, S., Joussaume, S., Peterchmitt, J.-Y., Abe-Ouchi, A., et al. (2007). Results of PMIP2 coupled simulations of the Mid-Holocene and Last Glacial Maximum - Part 1: experiments and large-scale features. *Climate of the Past*, 3, 261–277. <https://doi.org/10.5194/cp-3-261-2007>
- Brady, E. C., Otto-Bliesner, B. L., Kay, J. E., & Rosenbloom, N. (2013). Sensitivity to glacial forcing in the CCSM4. *Journal of Climate*, 26(6), 1901–1925. <https://doi.org/10.1175/JCLI-D-11-00416.1>
- Broecker, W., Bond, G., Klas, M., Clark, E., & McManus, J. (1992). Origin of the northern Atlantic's Heinrich events. *Climate Dynamics*, 6(3–4), 265–273. <https://doi.org/10.1007/BF00193540>
- Bryan, F. (1987). Parameter sensitivity of primitive equation ocean general circulation models. *Journal of Physical Oceanography*, 17(7), 970–985. [https://doi.org/10.1175/1520-0485\(1987\)017<0970:PSOPEO>2.0.CO;2](https://doi.org/10.1175/1520-0485(1987)017<0970:PSOPEO>2.0.CO;2)
- Bryan, K., & Lewis, L. J. (1979). Water mass model of the world ocean. *Journal of Geophysical Research-Oceans and Atmospheres*, 84(C5), 2503–2517. <https://doi.org/10.1029/JC084iC05p02503>
- Bryden, H. L., King, B. A., & McCarthy, G. D. (2011). South Atlantic overturning circulation at 24 S. *Journal of Marine Research*, 69(1), 38–55. <https://doi.org/10.1357/002224011798147633>
- Cheng, W., Weijer, W., Kim, W. M., Danabasoglu, G., Yeager, S. G., Gent, P. R., et al. (2018). Can the salt-advection feedback be detected in internal variability of the Atlantic Meridional Overturning Circulation? *Journal of Climate*, 31(16), 6649–6667. <https://doi.org/10.1175/JCLI-D-17-0825.1>
- Curry, W. B., & Oppo, D. W. (2005). Glacial water mass geometry and the distribution of $\delta^{13}\text{C}$ of ΣCO_2 in the western Atlantic Ocean. *Paleoceanography*, 20, PA1017. <https://doi.org/10.1029/2004PA001021>

- Dansgaard, W., Johnsen, S. J., Clausen, H. B., Dahl-Jensen, D., Gundestrup, N. S., Hammer, C. U., et al. (1993). Evidence for general instability of past climate from a 250-kyr ice-core record. *Nature*, 364(6434), 218–220. <https://doi.org/10.1038/364218a0>
- de Boer, A. M., Gnanadesikan, A., Edwards, N. R., & Watson, A. J. (2010). Meridional density gradients do not control the Atlantic Overturning Circulation. *Journal of Physical Oceanography*, 40(2), 368–380. <https://doi.org/10.1175/2009JPO4200.1>
- De Vries, P., & Weber, S. L. (2005). The Atlantic freshwater budget as a diagnostic for the existence of a stable shut down of the meridional overturning circulation. *Geophysical Research Letters*, 32, L09606. <https://doi.org/10.1029/2004GL021450>
- Delworth, T., & Mann, M. (2000). Observed and simulated multidecadal variability in the Northern Hemisphere. *Climate Dynamics*, 16(9), 661–676. <https://doi.org/10.1007/s003820000075>
- Drijfhout, S., Weber, S., & Swaluw, E. (2011). The stability of the MOC as diagnosed from model projections for pre-industrial, present and future climates. *Climate Dynamics*, 37(7–8), 1575–1586. <https://doi.org/10.1007/s00382-010-0930-z>
- Fanning, A. F., & Weaver, A. J. (1997). Temporal-geographical meltwater influences on the North Atlantic Conveyor: Implications for the Younger Dryas. *Paleoceanography*, 12(2), 307–320. <https://doi.org/10.1029/96PA03726>
- Fyke, J., & Eby, M. (2012). Comment on “Climate sensitivity estimated from temperature reconstructions of the Last Glacial Maximum”. *Science*, 337(6100), 1294. <https://doi.org/10.1126/science.1221371>
- Garzoli, S. L., Baringer, M. O., Dong, S., Perez, R. C., & Yao, Q. (2013). South Atlantic meridional fluxes. *Deep Sea Research, Part I*, 71, 21–32. <https://doi.org/10.1016/j.dsr.2012.09.003>
- Gent, P. (2018). A commentary on the Atlantic meridional overturning circulation stability in climate models. *Ocean Modelling*, 122, 57–66. <https://doi.org/10.1016/j.ocemod.2017.12.006>
- Gent, P. R. (2016). Effects of Southern Hemisphere wind changes on the Meridional Overturning Circulation in Ocean Models. *Annual Review of Marine Science*, 8(1), 79–94. <https://doi.org/10.1146/annurev-marine-122414-033929>
- Gent, P. R., & Danabasoglu, G. (2011). Response to increasing Southern Hemisphere winds in CCSM4. *Journal of Climate*, 24(19), 4992–4998. <https://doi.org/10.1175/JCLI-D-10-05011.1>
- Gent, P. R., & McWilliams, J. C. (1990). Isopycnal mixing in ocean circulation models. *Journal of Physical Oceanography*, 20(1), 150–155. [https://doi.org/10.1175/1520-0485\(1990\)020<0150:IMIOCM>2.0.CO;2](https://doi.org/10.1175/1520-0485(1990)020<0150:IMIOCM>2.0.CO;2)
- Gherardi, J.-M., Labeyrie, L., Nave, S., Francois, R., McManus, J. F., & Cortijo, E. (2009). Glacial-interglacial circulation changes inferred from $^{231}\text{Pa}/^{230}\text{Th}$ sedimentary record in the North Atlantic region. *Paleoceanography*, 24, PA2204. <https://doi.org/10.1029/2008PA001696>
- Gnanadesikan, A. (1999). A simple predictive model for the structure of the oceanic pycnocline. *Science*, 283(5410), 2077–2079. <https://doi.org/10.1126/science.283.5410.2077>
- Goes, M., Babcock, E., Bringas, F., Ortner, P., & Goni, G. (2017). The impact of improved thermistor calibration on the expendable bathythermograph profile data. *Journal of Atmospheric and Oceanic Technology*, 34(9), 1947–1961. <https://doi.org/10.1175/JTECH-D-17-0024.1>
- Goes, M., Christoffersen, J., Dong, S., Goni, G., & Baringer, M. O. (2018). An updated estimate of salinity for the Atlantic Ocean sector using temperature–salinity relationships. *Journal of Atmospheric and Oceanic Technology*, 35(9), 1771–1784. <https://doi.org/10.1175/JTECH-D-18-0029.1>
- Goes, M., Urban, N. M., Tonkonojenkov, R., Haran, M., Schmittner, A., & Keller, K. (2010). What is the skill of ocean tracers in reducing uncertainties about ocean diapycnal mixing and projections of the Atlantic Meridional Overturning Circulation? *Journal of Geophysical Research*, 115, C12006. <https://doi.org/10.1029/2010JC006407>
- Goes, M., Wainer, I., & Signorelli, N. (2014). Investigation of the causes of historical changes in the subsurface salinity minimum of the South Atlantic. *Journal of Geophysical Research: Oceans*, 119, 5654–5675. <https://doi.org/10.1002/2014JC009812>
- Gregory, J. M., Dixon, K. W., Stouffer, R. J., Weaver, A. J., Driesschaert, E., Eby, M., et al. (2005). A model intercomparison of changes in the Atlantic thermohaline circulation in response to increasing atmospheric CO₂ concentration. *Geophysical Research Letters*, 32, L12703. <https://doi.org/10.1029/2005GL023209>
- He, J., Winton, M., Vecchi, G., Jia, L., & Rugenstein, M. (2017). Transient climate sensitivity depends on base climate ocean circulation. *Journal of Climate*, 30(4), 1493–1504. <https://doi.org/10.1175/JCLI-D-16-0581.1>
- Hu, A. X., Meehl, G. A., Han, W. Q., Otto-Blistner, B., Abe-Ouchi, A., & Rosenbloom, N. (2015). Effects of the Bering Strait closure on AMOC and global climate under different background climates. *Progress in Oceanography*, 132, 174–196. <https://doi.org/10.1016/j.pocean.2014.02.004>
- Huisman, S. E., den Toom, M., Dijkstra, H. A., & Drijfhout, S. (2010). An indicator of the multiple equilibria regime of the Atlantic meridional overturning circulation. *Journal of Physical Oceanography*, 40(3), 551–567. <https://doi.org/10.1175/2009JPO4215.1>
- Ito, T., & Marshall, J. (2008). Control of lower-limb overturning circulation in the Southern Ocean by diapycnal mixing and mesoscale eddy transfer. *Journal of Physical Oceanography*, 38(12), 2832–2845. <https://doi.org/10.1175/2008JPO3878.1>
- Jansen, M. F. (2017). Glacial ocean circulation and stratification. *Proceedings of the National Academy of Sciences*, 114(1), 45–50. <https://doi.org/10.1073/pnas.1610438113>
- Kalnay, E., Kanamitsu, M., Kistler, R., Collins, W., Deaven, D., Gandin, L., et al. (1996). The NCEP/NCAR 40-year reanalysis project. *Bulletin of the American Meteorological Society*, 77(3), 437–471. [https://doi.org/10.1175/1520-0477\(1996\)077<0437:TNYRP>2.0.CO;2](https://doi.org/10.1175/1520-0477(1996)077<0437:TNYRP>2.0.CO;2)
- Klockmann, M., Mikolajewicz, U., & Marotzke, J. (2016). The effect of greenhouse gas concentrations and ice sheets on the glacial AMOC in a coupled climate model. *Climate Past*, 12(9), 1829–1846. <https://doi.org/10.5194/cp-12-1829-2016>
- Kohfeld, K., Graham, R. M., De Boer, A. M., Sime, L. C., Wolff, E. W., Le Quéré, C., & Bopp, L. (2013). Southern Hemisphere westerly wind changes during the Last Glacial Maximum: Paleo-data synthesis. *Quaternary Science Reviews*, 68, 76–95. <https://doi.org/10.1016/j.quascirev.2013.01.017>
- Kostov, Y., Armour, K. C., & Marshall, J. (2014). Impact of the Atlantic meridional overturning circulation on ocean heat storage and transient climate change. *Geophysical Research Letters*, 41, 2108–2116. <https://doi.org/10.1002/2013GL058998>
- Large, W., & Danabasoglu, G. (2006). Attribution and impacts of upper-ocean biases in CCSM3. *Journal of Climate*, 19(11), 2325–2346. <https://doi.org/10.1175/JCLI3740.1>
- Lee, S.-K., Lumpkin, R., Baringer, M. O., Meinen, C. S., Goes, M., Dong, S., et al. (2019). Global meridional overturning circulation inferred from a data-constrained ocean & sea-ice model. *Geophysical Research Letters*, 46, 1521–1530. <https://doi.org/10.1029/2018GL080940>
- Levermann, A., Mignot, J., Nawrath, S., & Rahmstorf, S. (2007). The role of Northern Sea Ice Cover for the weakening of the thermohaline circulation under global warming. *Journal of Climate*, 20(16), 4160–4171. <https://doi.org/10.1175/JCLI4232.1>
- Lippold, J., Luo, Y., Francois, R., Allen, S. E., Gherardi, J., Pichat, S., et al. (2012). Strength and geometry of the glacial Atlantic Meridional Overturning Circulation. *Nature Geoscience*, 5(11), 813–816. <https://doi.org/10.1038/ngeo1608>

- Liu, W., Liu, Z., & Brady, E. C. (2014). Why is the AMOC monostable in coupled general circulation models? *Journal of Climate*, 27(6), 2427–2443. <https://doi.org/10.1175/JCLI-D-13-00264.1>
- Liu, W., Liu, Z., Cheng, J., & Hu, H. (2014). On the stability of the Atlantic meridional overturning circulation during the last deglaciation. *Climate Dynamics*, 44(5–6), 1257–1275. <https://doi.org/10.1007/s00382-014-2153-1>
- Liu, W., Xie, S. P., Liu, Z., & Zhu, J. (2017). Overlooked possibility of a collapsed Atlantic meridional overturning circulation in warming climate. *Science Advances*, 3(1), e1601666–e1601666. <https://doi.org/10.1126/sciadv.1601666>
- Lumpkin, R., & Speer, K. (2007). Global ocean meridional overturning. *Journal of Physical Oceanography*, 37(10), 2550–2562. <https://doi.org/10.1175/JPO3130.1>
- Manabe, S., & Stouffer, R. J. (1988). Two stable equilibria of a coupled ocean–atmosphere model. *Journal of Climate*, 1(9), 841–866. [https://doi.org/10.1175/1520-0442\(1988\)001<0841:TSEOAC>2.0.CO;2](https://doi.org/10.1175/1520-0442(1988)001<0841:TSEOAC>2.0.CO;2)
- McManus, J. F., François, R., Gherardi, J. M., Keigwin, L. D., & Brown-Leger, S. (2004). Collapse and rapid resumption of Atlantic meridional circulation linked to deglacial climate changes. *Nature*, 428(6985), 834–837. <https://doi.org/10.1038/nature02494>
- Mecking, J. V., Drijfhout, S. S., Jackson, L. C., & Andrews, M. B. (2017). The effect of model bias on Atlantic freshwater transport and implications for AMOC bi-stability. *Tellus A*, 69, 1–14.
- Meissner, K., Weaver, A., Matthews, H., & Cox, P. (2003). The role of land surface dynamics in glacial inception: A study with the UVic Earth System Model. *Climate Dynamics*, 21(7–8), 515–537. <https://doi.org/10.1007/s00382-003-0352-2>
- Muglia, J., & Schmittner, A. (2015). Glacial Atlantic overturning increased by wind stress in climate models. *Geophysical Research Letters*, 42, 9862–9868. <https://doi.org/10.1002/2015GL064583>
- Muglia, J., Skinner, L. C., & Schmittner, A. (2018). Weak overturning circulation and high Southern Ocean nutrient utilization maximized glacial ocean carbon. *Earth and Planetary Science Letters*, 496, 47–56. <https://doi.org/10.1016/j.epsl.2018.05.038>
- Murphy, L. N., Goes, M., & Clement, A. C. (2017). The role of African dust in Atlantic climate during Heinrich events. *Paleoceanography*, 32, 1291–1308. <https://doi.org/10.1002/2017PA003150>
- Newsom, E. R., Bitz, C. M., Bryan, F. O., Abernathey, R., & Gent, P. R. (2016). Southern Ocean deep circulation and heat uptake in a high-resolution climate model. *Journal of Climate*, 29(7), 2597–2619. <https://doi.org/10.1175/JCLI-D-15-0513.1>
- Oka, A., Hasumi, H., & Abe-Ouchi, A. (2012). The thermal threshold of the Atlantic meridional overturning circulation and its control by wind stress forcing during glacial climate. *Geophysical Research Letters*, 39, L09709. <https://doi.org/10.1029/2012GL051421>
- Oppo, D. W., Curry, W. B., & McManus, J. F. (2015). What do benthic $\delta^{13}\text{C}$ and $\delta^{18}\text{O}$ data tell us about Atlantic circulation during Heinrich Stadial 1? *Paleoceanography*, 30, 353–368. <https://doi.org/10.1002/2014PA002667>
- Otto-Btiesner, B. L., & Brady, E. C. (2010). The sensitivity of the climate response to the magnitude and location of freshwater forcing: Last glacial maximum experiments. *Quaternary Science Reviews*, 29(1–2), 56–73. <https://doi.org/10.1016/j.quascirev.2009.07.004>
- Pacanowski, R. C. (1995). MOM 2 documentation: Users guide and reference manual, ver. 1.0. *Ocean Group Tech. Rep.* 3, Geophys. Fluid Dyn. Lab., Princeton, N. J.
- Rahmstorf, S. (1996). On the freshwater forcing and transport of the Atlantic thermohaline circulation. *Climate Dynamics*, 12(12), 799–811. <https://doi.org/10.1007/s003820050144>
- Roche, D. M., Paillard, D., Caley, T., & Waelbroeck, C. (2014). LGM hosing approach to Heinrich event 1: Results and perspectives from data-model integration using water isotopes. *Quaternary Science Reviews*, 106, 247–261. <https://doi.org/10.1016/j.quascirev.2014.07.020>
- Rugenstein, M. A., Winton, M., Stouffer, R. J., Griffies, S. M., & Hallberg, R. (2013). Northern High-Latitude Heat Budget Decomposition and Transient Warming. *Journal of Climate*, 26(2), 609–621. <https://doi.org/10.1175/JCLI-D-11-00695.1>
- Saenko, O. A. (2013). Projected strengthening of the Southern Ocean winds: Some implications for the deep ocean circulation. In A. Schmittner, J. C. Chiang, & S. R. Hemming (Eds.), *Ocean circulation: Mechanisms and impacts—Past and future changes of Meridional Overturning* (pp. 365–382). Washington, DC: American Geophysical Union. <https://doi.org/10.1029/173GM23>
- Saenko, O. A., Eby, M., & Weaver, A. J. (2004). The effect of sea-ice extent in the North Atlantic on the stability of the thermohaline circulation in global warming experiments. *Climate Dynamics*, 22(6–7), 689–699. <https://doi.org/10.1007/s00382-004-0414-0>
- Sarnthein, M., Winn, K., Jung, S. J. A., Duplessy, J.-C., Labeyrie, L., Erlenkeuser, H., & Ganssen, G. (1994). Changes in East Atlantic Deepwater Circulation over the last 30,000 years: Eight time slice reconstructions. *Paleoceanography*, 9(2), 209–267. <https://doi.org/10.1029/93PA03301>
- Sévellec, F., Fedorov, A. V., & Liu, W. (2017). Arctic sea-ice decline weakens the Atlantic Meridional Overturning Circulation. *Nature Climate Change*, 7(8), 604–610. <https://doi.org/10.1038/nclimate3353>
- Sherriff-Tadano, S., Abe-Ouchi, A., Yoshimori, M., Oka, A., & Chan, W. L. (2018). Influence of glacial ice sheets on the Atlantic meridional overturning circulation through surface wind change. *Climate Dynamics*, 50(7–8), 2881–2903. <https://doi.org/10.1007/s00382-017-3780-0>
- Sijp, W. P., & England, M. H. (2006). Sensitivity of the Atlantic thermohaline circulation and its stability to basin-scale variations in vertical mixing. *Journal of Climate*, 19(21), 5467–5478. <https://doi.org/10.1175/JCLI3909.1>
- Sime, L. C., Kohfeld, K. E., Le Quéré, C., Wolff, E. W., de Boer, A. M., Graham, R. M., & Bopp, L. (2013). Southern Hemisphere westerly wind changes during the Last Glacial Maximum: Model-data comparison. *Quaternary Science Reviews*, 64, 104–120. <https://doi.org/10.1016/j.quascirev.2012.12.008>
- Sloyan, B. M., & Rintoul, S. R. (2001). The Southern Ocean Limb of the Global Deep Overturning Circulation. *Journal of Physical Oceanography*, 31, 143–173. [https://doi.org/10.1175/1520-0485\(2001\)031<043:TSOLOT>2.0.CO;2](https://doi.org/10.1175/1520-0485(2001)031<043:TSOLOT>2.0.CO;2)
- Stommel, H. (1961). Thermohaline convection with two stable regimes of flow. *Tellus*, 13(2), 224–230. <https://doi.org/10.3402/tellusa.v13i2.9491>
- Talley, L. D. (2013). Closure of the global overturning circulation through the Indian, Pacific, and Southern Oceans: Schematics and transports. *Oceanography*, 26(1), 80–97. <https://doi.org/10.5670/oceanog.2013.07>
- te Raa, L. A., & Dijkstra, H. A. (2003). Sensitivity of North Atlantic multidecadal variability to freshwater flux forcing. *Journal of Climate*, 16(15), 2586–2601. [https://doi.org/10.1175/1520-0442\(2003\)016<2586:SONAMV>2.0.CO;2](https://doi.org/10.1175/1520-0442(2003)016<2586:SONAMV>2.0.CO;2)
- Toggweiler, J. R., & Samuels, B. (1993). In M. Heimann (Ed.), *Is the magnitude of the deep outflow from the Atlantic Ocean actually governed by Southern Hemisphere winds? The Global Carbon Cycle*. NATO ASI Series (Series I: Global Environmental Change), (Vol. 15). Berlin, Heidelberg: Springer.
- Wainer, I., Goes, M., Murphy, L. N., & Brady, E. (2012). Changes in the intermediate water mass formation rates in the global ocean for the Last Glacial Maximum, mid-Holocene and pre-industrial climates. *Paleoceanography*, 27, PA3101. <https://doi.org/10.1029/2012PA002290>
- Wang, C., Zhang, L., Lee, S.-K., Wu, L., & Mechoso, C. R. (2014). A global perspective on CMIP5 climate model biases. *Nature Climate Change*, 4, 2201–2205.

- Weaver, A. J., Eby, M., Kienast, M., & Saenko, O. A. (2007). Response of the Atlantic meridional overturning circulation to increasing atmospheric CO₂: Sensitivity to mean climate state. *Geophysical Research Letters*, 34, L05708. <https://doi.org/10.1029/2006GL028756>
- Weaver, A. J., Eby, M., Wiebe, E. C., Bitz, C. M., Duffy, P. B., Ewen, T. L., et al. (2001). The UVic Earth System Climate Model: Model description, climatology, and applications to past, present and future climates. *Atmosphere-Ocean*, 39(4), 361–428. <https://doi.org/10.1080/07055900.2001.9649686>
- Weber, S. L., & Drijfhout, S. S. (2007). Stability of the Atlantic Meridional Overturning Circulation in the Last Glacial Maximum climate. *Geophysical Research Letters*, 34, L22706. <https://doi.org/10.1029/2007GL031437>
- Weber, S. L., Drijfhout, S. S., Abe-Ouchi, A., Crucifix, M., Eby, M., Ganopolski, A., et al. (2007). The modern and glacial overturning circulation in the Atlantic ocean in PMIP coupled model simulations. *Climate Past*, 3(1), 51–64. <https://doi.org/10.5194/cp-3-51-2007>
- Weijs, W., de Ruijter, W. P., Dijkstra, H. A., & van Leeuwen, P. J. (1999). Impact of interbasin exchange on the Atlantic Overturning Circulation. *Journal of Physical Oceanography*, 29, 2266–2284. [https://doi.org/10.1175/1520-0485\(1999\)029<2266:IOEOT>2.0.CO;2](https://doi.org/10.1175/1520-0485(1999)029<2266:IOEOT>2.0.CO;2)
- Welander, P. (1986). Thermohaline Effects in the ocean circulation and related simple models. In J. Willebrand & D. L. T. Anderson (Eds.), *Large-scale transport processes in oceans and atmosphere, NATO ASI Series (Series C: Mathematical and Physical Sciences)* (Vol. 190, pp. 501–511). Dordrecht: Springer.
- Wright, D. G., & Stocker, T. F. (1991). A zonally averaged ocean model for the thermohaline circulation. Part I: Model development and flow dynamics. *Journal of Physical Oceanography*, 21(12), 1713–1724. [https://doi.org/10.1175/1520-0485\(1991\)021<1713:AZAOMF>2.0.CO;2](https://doi.org/10.1175/1520-0485(1991)021<1713:AZAOMF>2.0.CO;2)
- Xie, P., & Vallis, G. K. (2012). The passive and active nature of ocean heat uptake in idealized climate change experiments. *Climate Dynamics*, 38(3-4), 667–684. <https://doi.org/10.1007/s00382-011-1063-8>
- Zhang, J. (2014). Modeling the impact of wind intensification on Antarctic sea ice volume. *Journal of Climate*, 27(1), 202–214. <https://doi.org/10.1175/JCLI-D-12-00139.1>
- Zhang, R. (2008). Coherent surface-subsurface fingerprint of the Atlantic meridional overturning circulation. *Geophysical Research Letters*, 35, L20705. <https://doi.org/10.1029/2008GL035463>
- Zhu, J., Liu, Z., Zhang, X., Eisenman, I., & Liu, W. (2014). Linear weakening of the AMOC in response to receding glacial ice sheets in CCSM3. *Geophysical Research Letters*, 41, 6252–6258. <https://doi.org/10.1002/2014GL060891>